Characterizing the Spreading Behavior of Radius, Contact Angle, and Spreading Velocity of Trisiloxane "Superspreader" Surfactants

by

Sean K. Vaskov

Submitted to the
Department of Mechanical Engineering
in Partial Fulfillment of the Requirements for the Degree of

Bachelor of Science in Mechanical Engineering

at the

Massachusetts Institute of Technology

June 2012

Signature of author.....
Department of Mechanical Engineering
May 11, 2012

Certified by.....
Anette E. Hosoi
Associate Professor of Mechanical Engineering
Thesis Supervisor

Accepted by.....
John H. Lienhard V
Samuel C. Collins Professor of Mechanical Engineering
Undergraduate Officer

Characterizing the Spreading Behavior of Radius, Contact Angle, and Spreading Velocity of Trisiloxane "Superspreader" Surfactants

by

Sean K. Vaskov

Submitted to the Department of Mechanical Engineering
on May 11, 2012 in Partial Fulfillment of the
Requirements for the Degree of

Bachelor of Science in Mechanical Engineering

ABSTRACT

The ability of surfactants to lower surface tension makes them a key element in many products in a variety of industries. Trisiloxane surfactants have shown extraordinary wetting on hydrophobic surfaces, and are known as "superspreaders". Studies in the past have had inconsistent results characterizing the spreading of these surfactants. In this study, the radius and contact angle during spreading of different concentrations of trisiloxane ethoxylate are measured in a humidity-controlled box. Consistent with other studies, concentrations above the critical aggregation concentration spread more, resulting in lower contact angles and larger radii. The spreading behavior for radius and contact angle can be modeled using an exponential fit. Using the exponential models, a relationship between spreading velocity and contact angle can be found. For concentrations above the critical aggregation concentration, a linear relationship between contact angle and spreading velocity was found.

Thesis Supervisor: Anette E. Hosoi

Title: Associate Professor of Mechanical Engineering

Biographical Note

Sean Vaskov is a graduating senior majoring in mechanical engineering with a minor in engineering studies. He has a strong interest in the petroleum industry and has accepted a job at Shell Exploration and Production Company after graduation. His interest in the petroleum industry and the wide variety of applications for surfactants in it led him to focus his thesis on superspreaders.

Acknowledgements

The author would like to acknowledge Emilie Verneuil for help with designing the experimental setup, guidance for preparing and conducting tests and analyzing results. The author would also like to acknowledge professor Anette Hosoi for providing advice on how to best conduct experiments and analyze data, particularly with the software aspect of data analysis; as well as for providing guidance throughout the writing of this report.

Table of Contents

List of Figures

List of Tables

1. Introduction

1.1 Motivation: Surfactant Application to Petroleum Industry

Surfactants are compounds that lower the surface tension of a liquid, the interfacial tension between two liquids or the interfacial tension between a liquid and a solid. A variety of surfactants are used as wetting, cleaning, dispersing, emulsifying, foaming, and antifoaming agents in many products and industries. For example, in agriculture, surfactants can be added to fertilizer to improve the fertilizer's spreading ability on plants. Examples of other common products that benefit from the addition of surfactants are paints, detergents, fabric softeners, shampoos, inks and anti-fog solutions. In all applications, understanding the spreading properties of surfactants is useful in predicting their behavior and determining their employment.

Of particular interest are the applications of surfactants in the petroleum industry. Surfactants are used at all stages in the production process from drilling, reservoir management, oil well production, refinery processes, and transportation of petroleum emulsions. Specific applications of surfactants in the oil industry are shown in Table 1-1 (Schramm, 2000). Many of these applications take advantage of the unique surface interactions of surfactant solutions on hydrophobic substances.

Table 1-1: Some Examples of Surfactant Applications in the Petroleum Industry

Gas/Liquid Systems	Liquid/Liquid Systems	Liquid/Solid Systems
Producing oil well and wellhead foams	Emulsion drilling fluids	Reservoir wettability modifiers
Oil flotation process froth	Enhanced oil recovery in situ emulsions	Reservoir fines stabilizers
Distillation and fractionation tower foams	Oil sand flotation process slurry	Tank/vessel sludge dispersants
Fuel oil and jet fuel tank (truck) foams	Oil sand flotation process froths	Drilling mud dispersants
Foam drilling fluid	Wellhead emulsions	
Foam fracturing fluid	Fuel oil emulsions	
Foam acidizing fluid	Asphalt emulsion	
Blocking and diverting foams	Oil spill emulsions	
Gas-mobility control foams	Tanker bilge emulsions	

Two prevalent applications of surfactants are in the formation of foams and emulsions. The ability of a surfactant to reduce surface tension and contribute to surface elasticity is among the most important features of foam stabilization (Schramm, 2000). The use of surfactants in drilling foams leads to superior drilling penetration rates when compared to traditional mud systems. Such foams are often used in the drilling of horizontal wells to protect the reservoir from drill cuttings or to remove formation brine that enters wells when drilling. Foams are also injected into reservoirs to control the mobility of injected fluids. The recent shale gas boom has lead to the development of fracturing fluids. CO_2 based fluids are commonly used to fracture-stimulate formations with low reservoir pressure, as well as formations that are more sensitive to water treatments (high capillary pressure, swelling clays, etc.,) (Schlumberger, 2007). Viscoelastic, surfactant based CO_2 fluids with high foam quality are currently being considered and developed because they do not cause formation damage.

Emulsions are a mixture of oil and water, where one is suspended as drops in the other. In drilling, oil based and water based emulsions are often used as drilling fluid. Careful surfactant addition to these can minimize fluid loss into the reservoir, help cool and lubricate the drill bit, and help carry rock cuttings to the surface. In the recovery of bitumen from oil sands, surfactants are used to separate the bitumen particles from the sand and contain them so the sand particles can be recovered successfully. Surfactant selection to create the desired foam properties is important in both of these applications. In oil recovery, the capillary forces in porous rock or sand are responsible for retaining oil in a reservoir. Surfactant solutions can be used to reduce the capillary forces holding the oil and to alter the viscosity of the displacing fluid. The reduction of interfacial tensions allows for rapid emulsification of the oil into the surfactant solution, allowing for increased recovery.

1.2 Trisiloxane Surfactants and Superspreaders

Trisiloxane surfactants have been studied since the early 1990s and show total spreading on hydrophilic surfaces and extraordinary wetting on hydrophobic surfaces. These surfactants are commonly referred to as "superspreaders". Superspreading refers to droplets that spread until the contact angle between the drop and surface is zero. Surfactants consist of a hydrophobic head and a hydrophilic tail. The chemical structure of a trisiloxane molecule is shown in Figure 1-1. This structure is often denoted as $M(D'EO_nR)M$, where M represents the trimethylsiloxy group, $M= (CH_3)_3\text{-}SiO\text{-}$, the term $D'=\text{-}Si(CH_3)(R')\text{-}$, where $R'=(CH_2)_3$, onto which a poly(oxyethylene group, $EO_n=(CH_2CH_2O)_n$, is attached with n as the average number of poly(oxyethylene) groups. R stands for an end-capping group, usually $-H$,$-CH_3$, or $-C(O)CH_3$ (Radulovic, Sefaine, & Shanahan, 2009). The performance of trisiloxane molecules is often attributed to its T shape and large area of its hydrophobic head. These allow for the formation of unique aggregates within the fluid, which can influence wetting ability. Certain aggregates, such as vesicles, have been considered as a necessary condition for superspreading, although this has been questioned (Radulovic, Sefaine, & Shanahan, 2009).

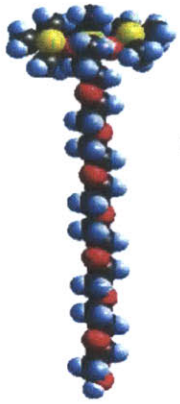

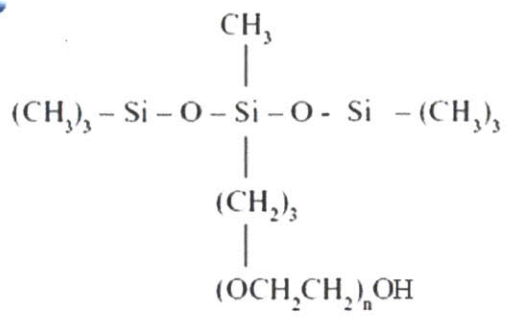

Figure 1-1: Molecular structure of trisiloxane surfactant. Red atoms are oxygen, black atoms are carbon, blue atoms are hydrogen, and yellow atoms are silicon. This surfactants performance is attributed to its T shape. (Radulovic, Sefaine, & Shanahan, 2009)

Wetting tests have been conducted to determine the optimal length of the hydrophobic tale. Trisiloxane molecules with an average of eight ethylene oxide groups provide superior wetting capability. The commercial superspreader Silwet L-77 has an average tail length of 7.5 groups and 80-85% concentration of active trisiloxane. Studies measuring the contact angle and drop radius while spreading have attempted to characterize the wetting behavior of trisiloxane surfactants. However, different studies have produced different time dependences for solutions of the same concentrations.

1.2.1 Critical Aggregation Concentration

The surface tension of a surfactant solution is dependent on the concentration of the surfactant. Increasing the concentration of surfactant drastically reduces the surface tension of the liquid, until the critical aggregation concentration is reached. Figure 1-2 visually outlines the effect of increasing concentration of a surfactant. When a small amount is added, surfactant molecules float freely around with some staying on the surface. Added surfactants form a layer of surfactants on the surface. The critical aggregation concentration is the point when the surfactant self associates in the liquid, after which any additional surfactants will form or join aggregates. For common surfactants these aggregates are typically micelles, however it is unclear if this is the only type of aggregate trisiloxane surfactants form.

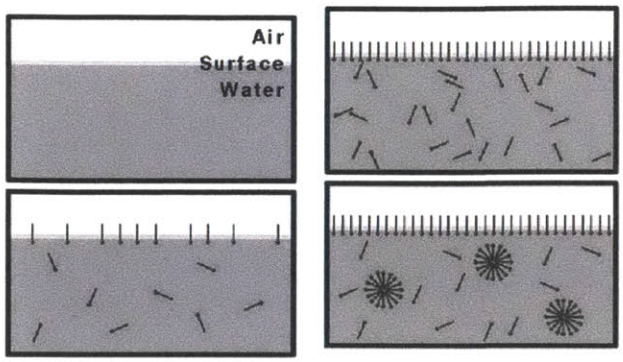

Figure 1-2: Depiction of increasing concentration of surfactants in water. Initially surfactants float freely, with some staying on the surface. Adding more forms a layer on the surface. The critical aggregation concentration is reached when the surfactant molecules self associate and any additional molecules form or join aggregates. The surface tension decreases with concentration until the critical aggregation concentration.
From: Wikipedia.org/Critical_micelle_concentration

The surface tension of a surfactant solution is dependent on the surfactant concentration. Figure 1-3 shows a plot of surface tension of Silwet L-77 solutions and surface tension. The critical aggregation concentration is around 0.01% where the surface tension levels off. The surface tension is the lowest between 0.1% and 1%; hence this region is called the "superspreading" region for the surfactant.

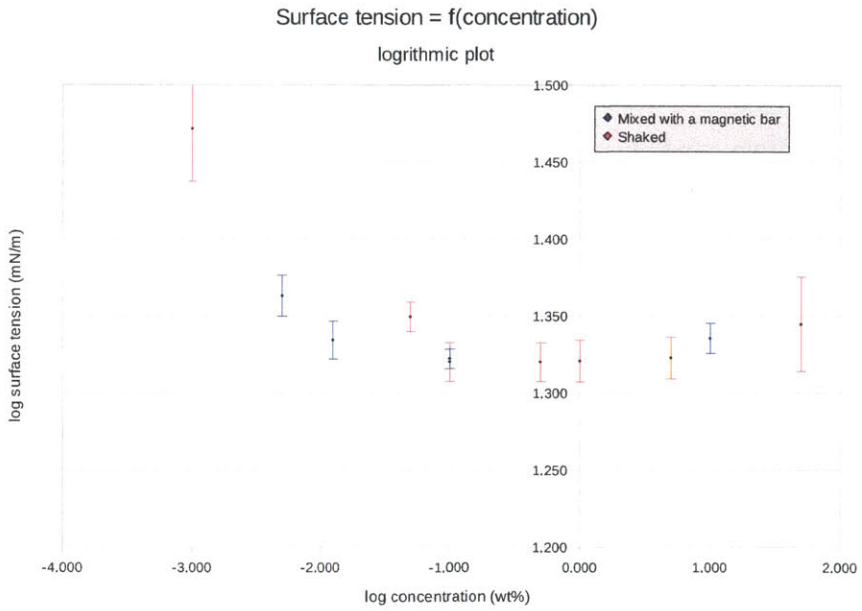

Figure 1-3: Plot of surface tension of Silwet L-77 solutions and surface tension. The critical aggregation concentration is around 0.01% where the surface tension levels off. The surface tension is the lowest between 0.1% and 1%; hence this region is called the "superspreading" region for the surfactant.

1.3 Spreading Theory

The spreading of a drop on a substrate is characterized by the spreading parameter. The spreading parameter is the difference in surface energy of the substrate when wet and dry and is defined in equation 1.

$$S = \gamma_{so} - (\gamma_{sl} + \gamma) \quad (1)$$

where γ_{so} is the surface tension between the substrate and environment, γ_{sl} is the surface tension between the substrate and liquid, and γ is the surface tension between the liquid and environment. A positive spreading parameter results in complete spreading of the drop to lower its surface energy. The result is a thin film spread evenly across the substrate. A negative spreading parameter results in partial wetting of the drop. The drop reaches an equilibrium point where all the surface tensions are balanced.

Small drops with negative spreading parameters have constant curvature and form a spherical cap with an equilibrium contact angle. Figure 1-4 shows a depiction of such a drop. The ability for a drop to form a spherical cap is dependent on the drops radius and capillary length. Drops where the radius is much smaller than the capillary length form spherical caps. Equation 2 estimates the capillary length (k^{-1}) of a fluid. The capillary length is a characteristic length above which gravity becomes important.

$$k^{-1} = \sqrt{\gamma/\rho g} \quad (2)$$

where ρ is the density of the fluid, and g is the acceleration due to gravity.

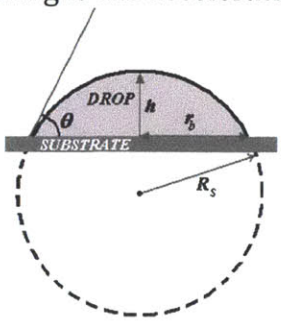

Figure 1-4: Depiction of a drop forming a spherical cap on a substrate. Drops form spherical caps when their radius is much less than their capillary length. Image from: http://www.sciencedirect.com

The driving force for the drop wetting the surface can be found from the surface tension, current contact angle (θ), and equilibrium contact angle (θ_e). Equation 4 defines the driving force for the drop to wet the surface as:

$$F = \gamma(\cos\theta - \cos\theta_E) \quad (4)$$

The friction force opposing the movement is given in equation 5 (Radulovic, Sefaine, & Shanahan, 2009):

$$F_f = \frac{3\eta l V}{\theta} \quad (5)$$

where η is the liquid's viscosity, V is the spreading velocity, and l is the logarithm of the ratio of the size of the drop to the liquid's molecular size. A drop spreads until the friction force is balanced with the driving force.

1.4 Literature Review

Different studies on superspreaders have pointed to different techniques to model spreading. It has been observed that the maximum spreading appears in a narrow concentration region of 0.4%wt-0.6%wt (Nikolov & Wasan, 2011). This observation for a less-concentration-dependent sample on the maximum of the spreading rate vs. the substrate wettability suggests that the absorption of the solid/liquid interface may not be the main factor in the rate of spreading; the air/liquid surface tension may be a more important factor for spreading models.

Based on data analysis, a simple model was used to predict the rate of radial spreading. A power law for liquid spreading on a solid was derived by Tanner and later Gennes (Nikolov & Wasan, 2011). The power law proposes the radius as function of time in the form $R(t)=Ct^{\alpha}$ where C and α are spreading parameters. Although this model has fit data in the past well, the physical meaning for parameters C and α are still unclear. A graph showing exponents for the wetting of 0.1%wt solution vs the hydrophobicity of the substrate is shown in Figure 1-5. Table 1-2 displays the spreading exponents, contact angle of water, substrate, and origin of data for each point in Figure 1-5. From this graph it is clear that the hydrophobicity of the substrate has a significant effect on the spreading characteristics of the solution.

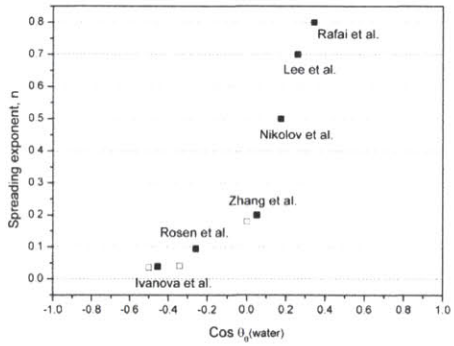

Figure 1-5: Plot of spreading exponents estimated by fit to $r \sim t^n$ power law for 0.1% wt drops. Shown as a function of the equilibrium contact angle of water for the substrate. (Radulovic, Sefaine, & Shanahan, 2009)

Table 1-2: Values and Origin of Reported Wetting Exponents, Together with the Corresponding List of Substrates on Which the Wetting of 0.1%wt Trisiloxane Solution Was Investigated (Radulovic, Sefaine, & Shanahan, 2009)

Wetting exponent	Water contact angle (°)	Substrate	Origin of data/publication
0.8	70	PET	Rafai et al. (2002)
0.7	75	PS	Lee et al. (2008)
0.5	80	PS	Nikolov et al. (2002)
0.2	87	Cabbage	Zhang et al. (2006)
0.18	90	Parylene	Radulovic et al. (2009)
0.095	105	Parafilm	Rosen et al. (1996)
0.041	110	Cytop	Radulovic et al. (2009)
0.039	117	PTFE AF	Ivanova et al. (2009)
0.036	120	Teflon	Radulovic et al. (2009)

Later studies proposed an exponential model for spreading, where the wetting is divided into three stages. The initial stage is characterized by a sharp increase in drop radius and decrease of contact angle. The intermediate stage shows a relatively moderate increase in drop radius, followed by an exponential relaxation at the end of the wetting process (Radulovic, Sefaine, & Shanahan, 2009). The study proposes that equations 4 and 5 can be combined to model the equilibrium state, shown in equation 6.

$$F = \frac{3\eta l}{\theta}\frac{dr}{dt} = \gamma(cos\theta_e - cos\theta(t)) \quad (6)$$

Equation 6 can be linearized with the time constant $T=\eta l r_e/(\gamma\theta_e^3)$ to obtain equations 7 and 8 for the radius and contact angle respectively:

$$r(t) = r_e - a * \exp\left(-\frac{t}{\tau_r}\right) \quad (7)$$

$$\theta(t) = \theta_e + b * \exp\left(-\frac{t}{\tau_\theta}\right) \quad (8)$$

The exponential model proposed by Radulovic fits data for substrates of lower hydrophobicity, but its fit for substrates with higher hydrophobicity is questionable. For spreading on hydrophobic substrates, the intermediate stage is less apparent. The goal of this study is to examine the spreading of different trisiloxane solutions on substrates with high hydrophobicity. In addition, previous studies have had the drops fall from distances of approximately 1cm. This may add additional inertial effects to the spreading of the drop. This study will eliminate free falling of the drop to reduce inertial effects. Finally, this study will conduct experiments in a humidity-controlled box to minimize the effects of evaporation.

2. Experimental Design

To record the spreading of solutions, the drop radius and contact angle were measured via imaging using a Thorlabs camera. The camera is connected to a computer, which records video sequences. In order to control humidity, the drops were deposited in an airtight acrylic box, shown in Figure 2-1. The acrylic used for the box is 0.236" thick and bound using acrylic solvent. High vacuum silicon grease was used to seal the edges of the top and front; which needed to be opened and closed to change substrates and salts. Outside lighting was reflected off white paper to allow for proper imaging of the drop. Paper was placed on top of the box to improve imaging of the drops on reflective silicone.

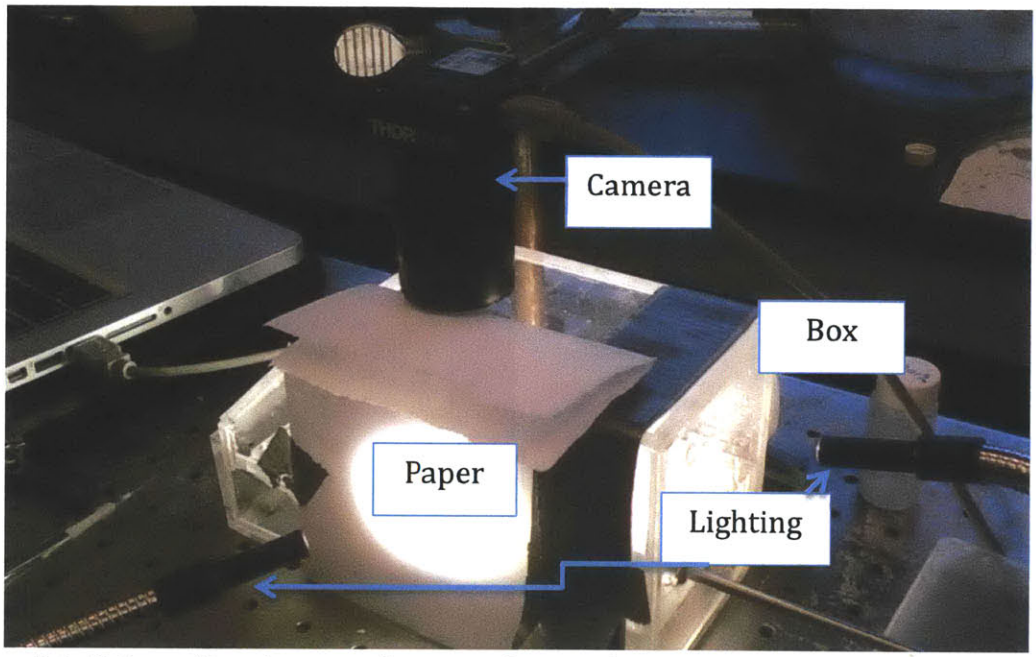

Figure 2-1: Set up of box for spreading experiments. A camera captures images of the drop in a humidity-controlled box.

The inside of the box as viewed by the camera is shown in Figure 2-2. The substrate is located on a platform with a slider to allow for imaging multiple samples. A prism is placed next to the substrate. The prism displays the side image of the drop, allowing for the radius and contact angle to be imaged simultaneously from the top. A platform with holes to allow for air circulation supports both the prism and substrate. The salts used to control humidity are placed beneath the platform. The drops are injected using a VWR pipette capable of depositing drops 2-20 μL with a resolution of 0.1 μL. The pipette enters the box through a hole oriented 45° to the substrate.

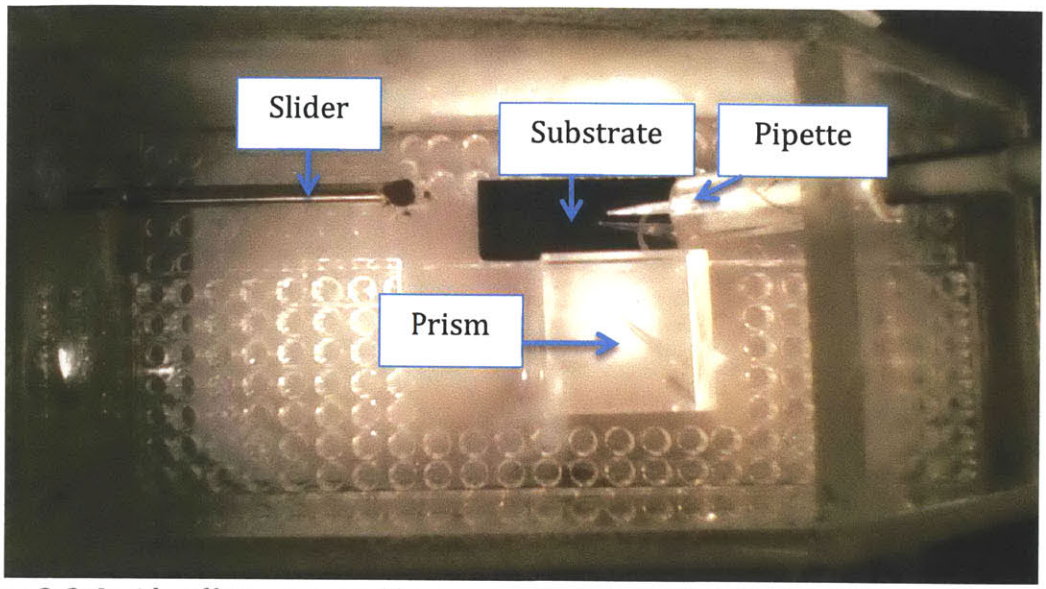

Figure 2-2: Inside of box as viewed by camera. Drops are deposited on substrate by a pipette. A prism next to the substrate allows for the camera to capture the top and side view of the drop simultaneously. A slider allows for multiple samples to be taken without opening the box. The salts are placed in trays at the bottom of the box.

The substrate used for these experiments is silicon with a hydrophobic coat. The silicon was chosen for its smooth surface and high hydrophobicity. The contact angle of water on the silicone was 102±5°.

In order to cover all ranges of surface tension measured in Figure 3, concentrations of 0.0001%, 0.001%, 0.01%, 0.1%, 1%, and 10% wt of Silwett L-77 to water were mixed. The surfactant was manually dissolved in water for each solution.

The bottom of the box contains a tray in which salt solutions are placed. The salt solutions allow for the humidity to be controlled at specific levels. Table 2-1 shows prepared salts and the relative humidity they correspond to.

Table 2-1: Salt solutions and their relative humidities

Salt	Humidity (at 25°C)
K_2CO_3, $1.5H_2O$	43.2%
NaCl	75.4%
K_2SO_4	97.0%

Prior to imaging drops the humidity of the box was checked. Four supersaturated salts were prepared. Each salt was dissolved in water. The mixture was then raised to 80°C where more salt was added and dissolved. The mixture was then brought down to room temperature. Each mixture was made to obtain about 200ml of saturated solution and 100ml of undissolved salt. A VWR humidity sensor capable of reading relative humidity 25-98% at a resolution of 2%, was placed inside the box. Each salt was placed in the tray and the time for the humidity to

reach equilibrium was measured. Equilibrium for all salts was reached within 12 hours.

2.1 Testing Procedure

Three 5 μL drops of each concentration were tested. The salt solution used was K_2CO_3, $1.5H_2O$, which recorded an equilibrium humidity of 40±2%. The substrate and salt were placed in the box, and the pipette hole was plugged with rubber overnight to allow the humidity to equilibrate. Each drop was deposited using the pipette. The pipette tip was held as close to the substrate as possible to minimize inertial effects. After depositing the drop, the pipette was removed and the hole plugged to minimize evaporation. The videos were analyzed in Matlab using a program that measures the radius and contact angle of the drops. Videos were taken with speeds of 115-122 frames per second in order to accurately capture the initial spreading process.

3. Data Analysis

3.1 Extracting Drop Radius and Contact Angle from Video

A Matlab code was written to extract the contact angle and drop radius from spreading videos captured with the camera. The Matlab code works by detecting circles in the image for the top and side view of the drop. The contact angle is calculated using the radius of the circle, drop height, and baseline. A line is detected for the base for the prism. Figure 3-1 shows a sample image from the camera, with the circles and lines detected by Matlab. The original image is split into an image of the top view from which radius is measured (left) and the side view from which contact angle is measured (right). The code analyzes each image separately for each frame. The code works in reverse by finding the radius of the drops after spreading. Using the final radius, the program steps back through the frames, tightening the radius range of the circles appropriately, allowing for Matlab to detect circles in a narrow radius range. The Matlab code is included in the Appendix.

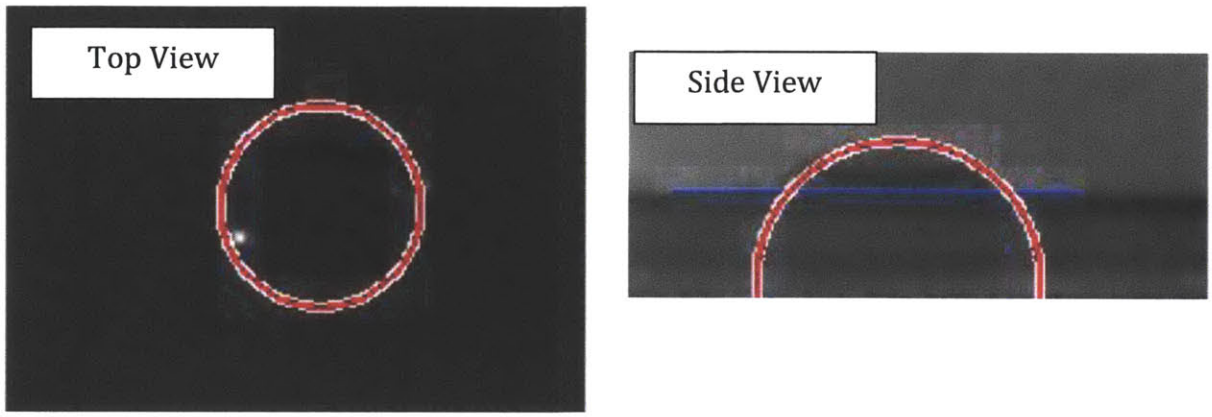

Figure 3-1: Sample image of analysis done in Matlab. The image on the left shows the top view from which radius is measured, and the image on the right shows the bottom view from which contact angle is measured. The code detects circles for the top and side views of the drop, and a line for the base of the prism. The contact angle is calculated using the radius of the circle, drop height, and baseline.

3.2 Data Analysis Techniques

The data gathered from the Matlab code was inconsistent. Multiple trials for each concentration often showed different spreading behavior. The role of human error in holding the pipette may have led to this inconsistency. During analysis of data, the circle detection often shifted circles based on shadows and miscellaneous features in some frames. To resolve inconsistencies, a moving average was applied to data sets to smooth out errors. For the quick initial spreading, a moving average of 4 frames was taken. For the end phase, a moving average of 10 frames was taken. Figure 3-2 shows an example plot of the original data (top) compared to a plot of data with a moving average applied (bottom) for a surfactant concentration of 1%.

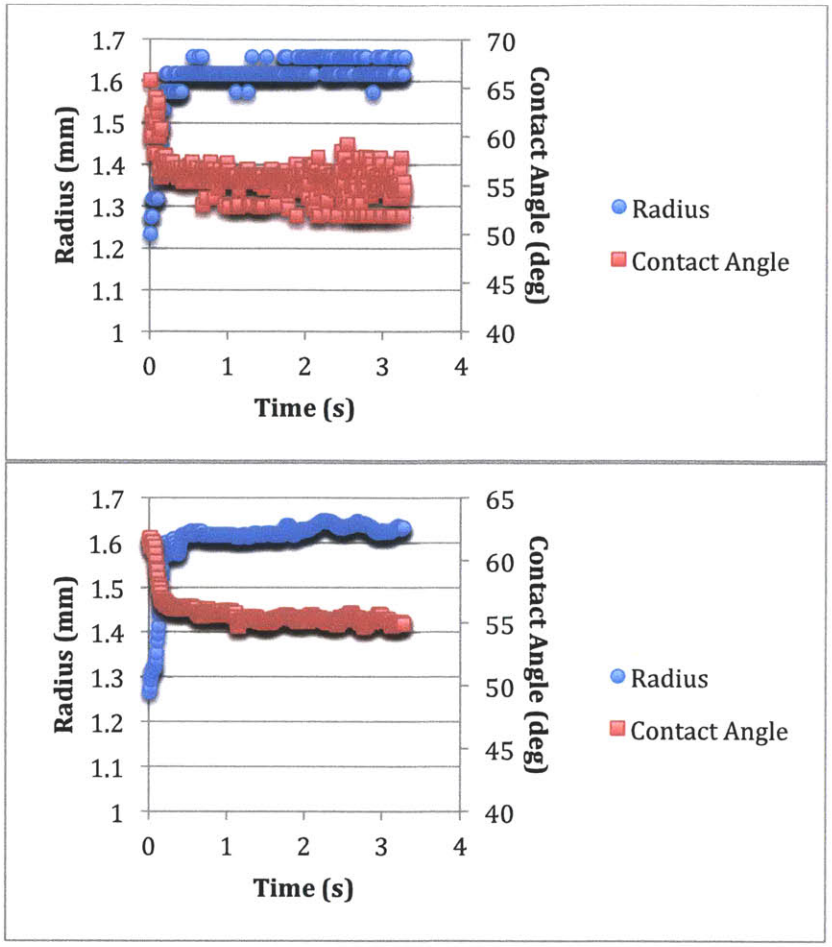

Figure 3-2: Comparison of data before and after a moving average is applied. The top chart shows the original data collected from Matlab, and the bottom data shows that data with a moving average applied.

Another difficulty encountered during testing was the formation of capillaries between the pipette and substrate, particularly for solutions with lower surfactant concentrations. Figure 3-3 shows a sample image of this type of capillary. Although, some spreading was observed during this phase, the contact angle was not measurable using the above method because the drop had yet to form a spherical cap. The capillary formation limited the timespan of accurate data that could be acquired.

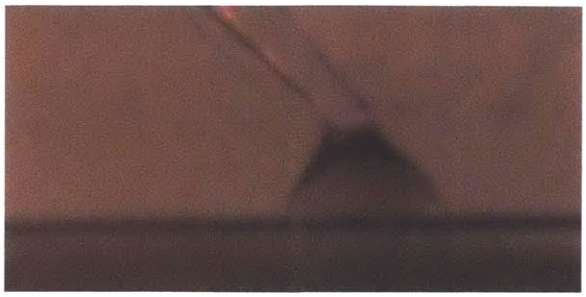

Figure 3-3: Sample image of capillary forming between pipette and substrate.

After applying a moving average to all data sets and removing sections with capillaries, the data was analyzed using a variety of fitting techniques. In all data sets for radial spreading, the initial wetting phase (between 0 and 0.5 seconds) was analyzed. For contact angle, the initial wetting phase was between 0 and 0.3 seconds.

In an attempt to fit data to equations described in the literature review above, a Matlab script was used. The Matlab script works by selecting coefficients and minimizing the sum of the error squared for each point. Using this Matlab script, it was found that the exponential models described in equations and 7 and 8 fit the data better than the power law derived by Tanner. Figure 3-4 shows a plot of sample data with exponential and power fits. The points are data for radius with a concentration of 0.1%wt Silwet L-77. The exponential fit is the black line, and the power law is the red dotted line. The exponential fit characterizes the spreading behavior better than the power law.

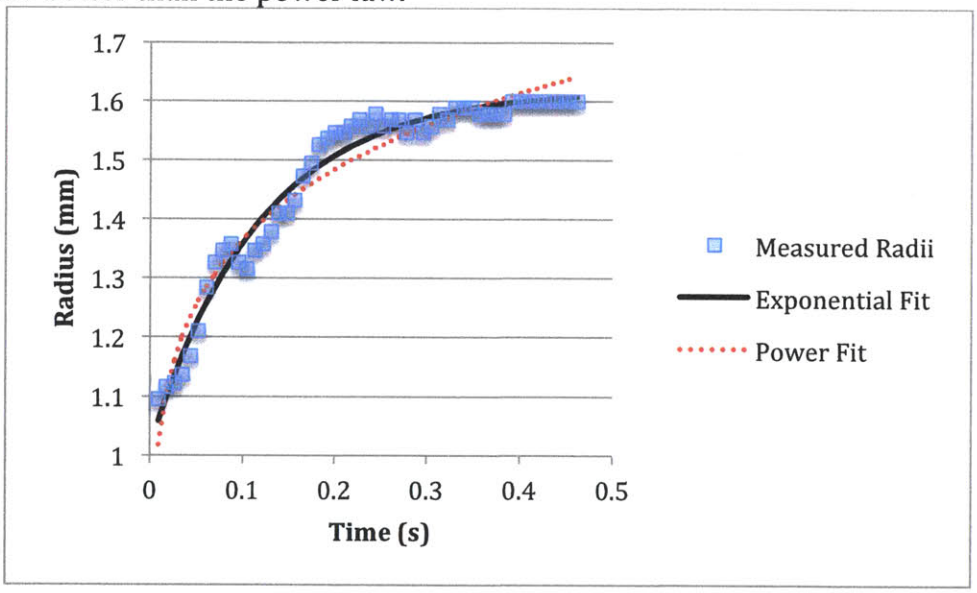

Figure 3-4: Comparison of exponential fit and power law for radius with respect to time. The exponential fit is marked with a black line, and the power law is marked with a red dotted line. The exponential fit models the spreading behavior better.

4. Discussion

The equilibrium results found are consistent with the spreading theory and behavior observed in other studies. Solutions with low surfactant concentrations, displayed less spreading, and had higher contact angles and smaller radii. Solutions with concentrations of 0.1%, 1%, and 10% had the lowest contact angles and highest radii, consistent with the fact that those concentrations are above the critical aggregation concentration and have low surface tensions. Figures 4-1 and 4-2 respectively show plots of final radius and contact angle as a function of surfactant concentration. The measured error for final radius was ±0.1mm, and for final contact angle ±5°. Interestingly, the final contact angle for a surfactant concentration 0.001% was slightly higher than for pure water (108±5° compared to 102±5°). This indicates that at concentrations this low, the addition of surfactants has little effect on spreading.

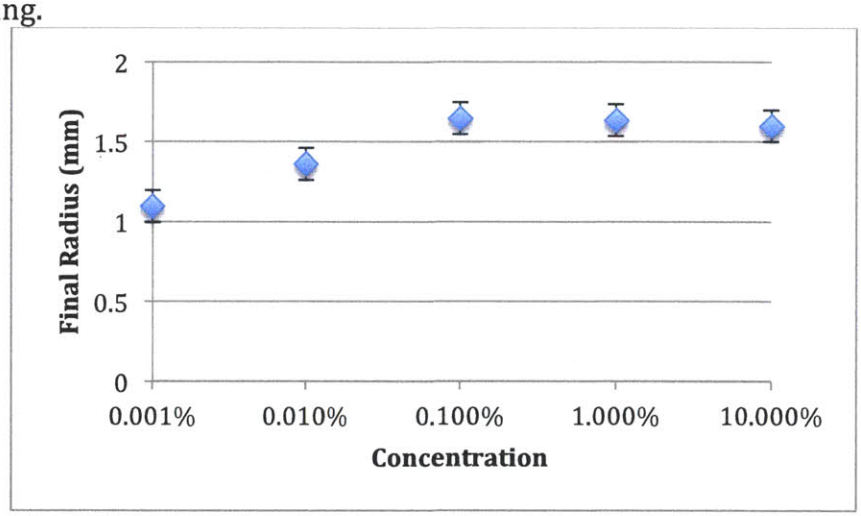

Figure 4-1: Plot of final radius vs surfactant concentration. The highest radii occur above the critical aggregation concentration.

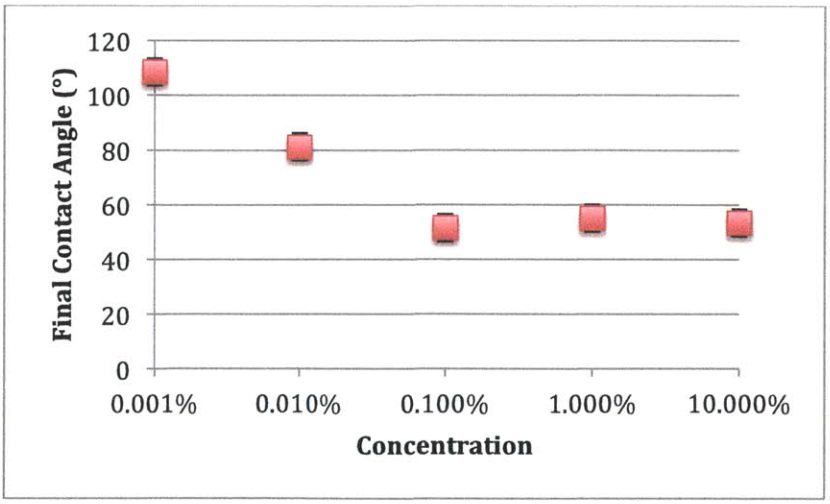

Figure 4-2: Plot of final contact angle vs surfactant concentration. The lowest contact angles occur at concentrations at or greater than 0.1%, indicating the surfactant has reached the critical aggregation concentration.

4.1 Spreading Behavior

The initial radial spreading can be modeled exponential as described in equation 7, copied below:

$$r(t) = r_e - a * \exp\left(-\frac{t}{\tau_r}\right) \quad (7)$$

Figure 4-3 shows a plot of radius as a function of time with the corresponding exponential fits. As expected, solutions above the critical aggregation concentration spread to a larger radius than that below. Table 4-1 gives the coefficients found by fitting. For radial spreading, concentration 0.001%wt is not plotted because it did not spread enough for valuable data to be collected.

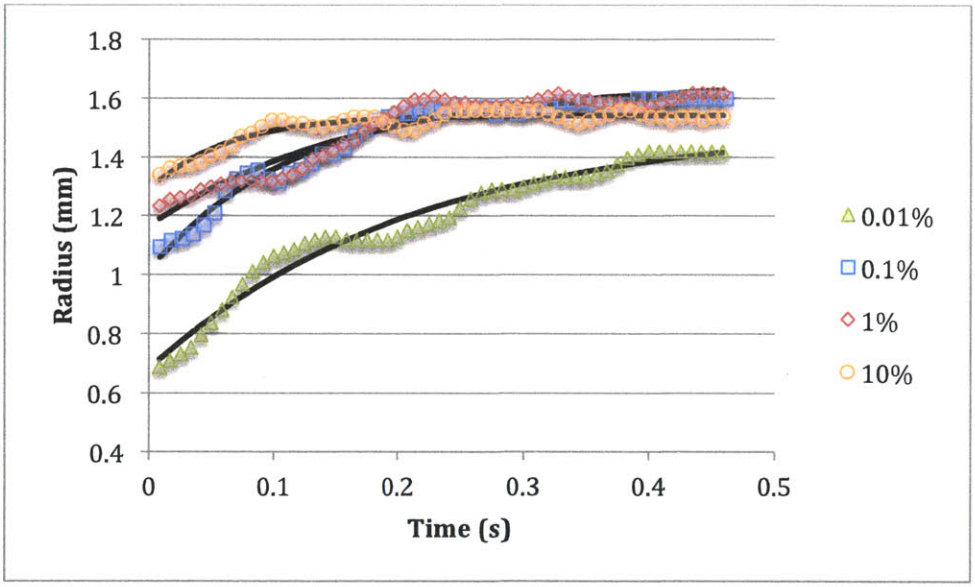

Figure 4-3: Plot of radius as a function of time for concentrations 0.01%,0.1%,1%, and 10% wt Silwet L-77. The black lines plotted are exponential fits for each concentration.

Table 4-1: Coefficients for Exponential Fits of Radial Spreading

Concentration	r_e (mm)	a (mm)	T_r (s)
0.01%	1.5147	0.833	0.2143
0.1%	1.6207	0.6047	0.1191
1%	1.6595	0.4929	0.1683
10%	1.5431	0.2509	0.0634

As expected, solutions above the critical aggregation concentration spread quicker than those below. The time constants (τ_r) for concentrations 0.1%, 1%, and 10% are significantly lower than the time constant for 0.01%. Interestingly, the amount of spreading between the initial radius and final radius (characterized by the coefficient a) decreases as concentration increases. This decrease can be attributed to higher concentrations having higher initial radii. A different method of depositing drops, in order to ensure they all start at the same radius should be investigated in future research.

Similar to radial spreading, the decrease in contact angle can also be modeled exponentially as described in equation 8, copied below:

$$\theta(t) = \theta_e + b * \exp\left(-\frac{t}{\tau_\theta}\right) \quad (8)$$

Figure 4-4 shows a plot of contact angle as a function of time with corresponding exponential fits. As expected solutions above the critical aggregation concentration settle at a lower contact angle than those below. Table 4-2 gives the coefficients found by fitting.

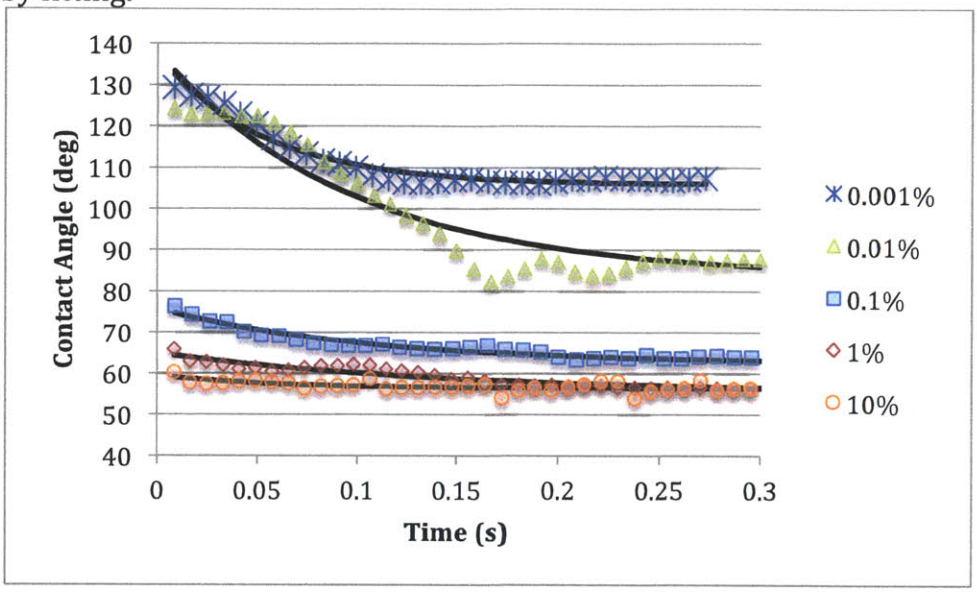

Figure 4-4: Plot of contact angle as a function of time. The black lines plotted are exponential fits for each concentration.

Table 4-2: Coefficients of Exponential Fits for Contact Angle

Concentration	θ_e (deg)	b (deg)	τ_θ (s)
0.001%	105.804	31.1499	0.0532
0.01%	83.5319	54.2384	0.0964
0.1%	62.3262	13.4058	0.1041
1%	55.3674	9.3993	0.1454
10%	56.2430	3.0982	0.0536

Surprisingly, there appears to be little relationship between the time constants for contact angle (τ_θ) and concentration. It is expected that solutions below the critical aggregation concentration would have larger time constants because they spread slower. It is also surprising that for 0.01%, the time constant for contact angle (0.0964) is much less than that for radius (0.2143). For higher concentrations the time constants are similar, indicating an expected relationship between radial spreading and contact angle. The coefficient b indicates the amount of reduction in contact angle. This coefficient decreases with contact angle, indicating that solutions of higher concentrations initially started at lower contact angles than those of lower concentrations.

4.2 Spreading Velocity

The spreading velocity (defined as the increase in radius over time) can be related to the contact angle. Equation 9 defines the contact angle as a function of spreading velocity (v) by taking the derivative of equation 7 and combining it with equation 8:

$$\theta(v) = \theta_e + b\left(\frac{\tau_r}{a}v\right)^{\frac{\tau_r}{\tau_\theta}} \tag{9}$$

For solutions where the time constants for radial spreading and contact angle reduction are approximately equal, the equation can be linearized as:

$$\theta(v) = \theta_e + \frac{b\tau_r}{a}v \tag{10}$$

Figure 4-5 shows a plot of contact angle as a function of spreading velocity. Velocity is found by taking the derivative of the exponential fit for radial spreading for each concentration. Concentrations with similar time constants for radial spreading and contact angle reduction were chosen to show a linear relationship between contact angle and velocity. The black lines in the plot are for the fit described in equation 9.

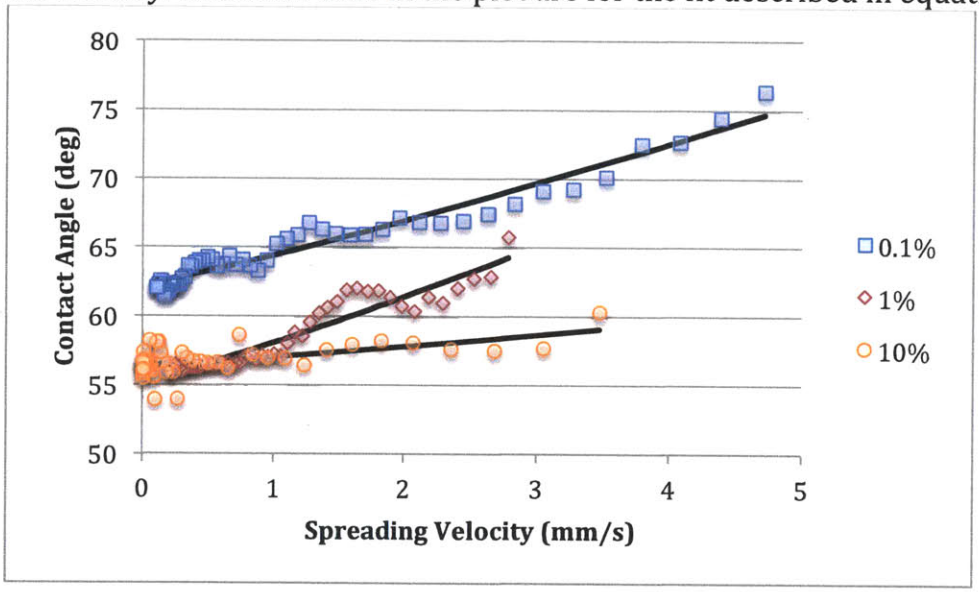

Figure 4-5: Plot of contact angle as a function of velocity for concentrations 0.1%,1%, and 10%. The black lines plotted represent fits found using equation 9.

Figure 4-5 shows that for the plotted concentrations, a linear relationship between velocity and contact angle can be approximated. Table 4-3 gives the theoretical coefficients for the linear equation described in equation 10 (θ_e and $\frac{b\tau_r}{a}$) compared to those found using a linear fit (B and m respectively). The similarity between the theoretical coefficients to those found with a linear fit shows that the relationship between contact angle and spreading velocity can be modeled linearly.

Table 4-3: Coefficients of Linear Fit for Contact Angle as a Function of Velocity

Concentration	θ_e (deg)	$\frac{b\tau_r}{a}$ (deg*s/mm)	B (deg)	m (deg*s/mm)
0.1%	62.3262	2.6404	61.997	2.5826
1%	55.3674	3.2094	54.987	3.2172
10%	56.2430	0.7829	56.38	0.7313

4.3 Conclusion

The equilibrium radii and contact angle follow trends consistent with previous studies. Concentrations above the critical aggregation concentration have the largest radii and lowest contact angles. The spreading behavior of radius and contact angle for surfactant solutions can be modeled using exponential functions. It is expected that time constants for concentrations above the critical aggregation concentration will be lower than those for concentrations below. However, in this experiment, time constants for contact angle reduction were lower for concentrations below the critical aggregation concentration. Experiments using a different method of depositing solutions should be conducted to figure out whether or not this phenomenon is a result of human error. Using the exponential fits, a relationship between spreading velocity and contact angle can be found. For concentrations with similar time constants for contact angle and radius, the relationship between velocity and contact angle can be modeled with a linear function.

5. Appendices

Appendix A: Matlab code for video analysis

The matlab code for video analysis consists of 2 scripts and 2 functions. The script video analysis is the main script used to take a video and calculate the radius and contact angle for all of its frames. The function dropinfo is called by video analysis to return the radius and contact angle of each frame. The function contact angle is called by dropinfo to calculate the contact angle for each frame. The script image analysis is used to produce an image of the side view of the drop with lines detected to allow for the base of the prism to be found (entered in video analysis and used to calculate contact angle).

Video Analysis

Purpose: to analyze the video frame by frame and store values for radius and contact angle

```
clear

%video reader object
dropvideo=VideoReader('k2c03_1%_coatedsi_4.avi'); %name of video file
start=642;%initial frame
stop=643;%final frame
p=stop-start;

radii=zeros(p,1);
theta=zeros(p,1);

%get information
lastradius=39;%radius of drop at final frame
lasttopcenter=[52.9829   52.8366]; %center of drop at final frame
lastsideradius=55; %radius of cricle detected for side view at final
frame
lastsidecenter=[56    3]; %center of circle detected for side view a
final frame
base=32; %pixel (vertical) for base of prism
for i=1:p
    d=start+(p-(i-1));
    index=p-(i-1);
    img = read(dropvideo,d);

[radii(index),c,theta(index),sr,sc]=dropinfo(img,lastradius,lasttopcent
er,lastsideradius,lastsidecenter,base);
    lastradius=radii(index);
    lastopcenter=c;
    lastsideradius=sr;
    lastsidecenter=[sc(1) sc(2)+sr];
end
```

Drop Info

Purpose: to find the radius and contact angle of an image of a drop

```
function [radius,topcenter,theta,sideradius,sidecenter] =
dropinfo(image,lastradius,lasttopcenter,lastsideradius,lastsidecenter,b
ase)
%takes image file, finds drop radii and contact angle
%image is the image, pixel is the pixels for 1mm, lastr is radius(mm)
of the
%last image lastrt is the radius of the side view (mm)
%dropcenter is the center of the last top view
%side center is the center of the last side view

%convert to black and white
I=rgb2gray(image);
Itop=I(50:150;50:150);%portion of image containing top view
Ibottom=I(200:300,50:10);%portion of image containing side view

%find circles centers, radii, and metric
maxr=int16(round(lastradius)*1.02);
minr=int16(round(lastradius*.95));
BW=edge(Itop,'canny');
[centers,radii,metric]=imfindcircles(BW,[minr
maxr],'ObjectPolarity','dark','Method','TwoStage','EdgeThreshold',0,'Se
nsitivity',0.98);
no=size(centers);
if(no==0)
    radius=lastradius;
    topcenter=lasttopcenter;
else
    [M,ix]=max(metric);
    index=ix;
    radius=radii(index);
    topcenter=centers(index,:);
end

%contact angle
BW2=edge(Ibottom,'canny');
maxrt=int16(round(lastsideradius)*1.05);
minrt=int16(round(lastsideradius)*.85);
[centerst,radiit,metrict]=imfindcircles(BW2,[minrt
maxrt],'ObjectPolarity','dark','Method','TwoStage','EdgeThreshold',0,'S
ensitivity',1 );
n=size(centerst);
[M,ix]=max(metrict);
indext=ix;
sidecenter=centerst(indext,:)
sideradius=radiit(indext)
%calculate contact angle
theta=contactangle(centerst(indext,2),radiit(indext),base);
end
```

Contact Angle

Purpose: to calculate the contact angle given radius and center of the fitted circle and position of the prism

```
function [theta] = contactangle(centery,r,y2)
%find the contact angle between a circle and a line
%centery is the center y point of cirlce, r is radius, y2 is y of line
adj=y2-centery;
temp=acos(adj/r);
t=temp;
theta=180/pi*t;
end
```

Image Analysis

Purpose: to analyze a frame of the video to find the position of the prism base

```
RGB=read(VideoReader('k2c03_1%_coatedsi_4.avi'),200);%image frame from
video
%convert to black and white
I=rgb2gray(RGB);
[row,column]=size(I);
Ibottom=I(53:101,265:359);%portion of image containing side view

%find baseline
%extract edges
BW=edge(Ibottom,'canny');
[H,T,R]=hough(BW,'RhoResolution',0.5,'Theta',-90:0.5:89.5);
P=houghpeaks(H,200,'Threshold',20);
linesL = houghlines(BW,T,R,P,'MinLength',5,'Fillgap',5);
figure, imshow(BW), hold on

%display lines
for k = 1:length(linesL)
   xy = [linesL(k).point1; linesL(k).point2];
   plot(xy(:,1),xy(:,2),'LineWidth',2,'Color','blue');

end
```

Appendix B: Matlab code for exponential and power law fitting

Exponential Fit for Radius

Function expfitradius returns the sum of error squared for coefficients

```
function [sse] = expfitradius(params,Input,Actual_Output)
%fit of radius data to exponential function r(t)=re-a*exp(-t/T)
%params should be an array of the form params=[re a T]
re=params(1);
a=params(2);
T=params(3);
Fitted_Curve=re-a.*exp(-1/T*Input);
Error_Vector=Fitted_Curve-Actual_Output;
%sum of squares error
sse=sum(Error_Vector.^2);
end
```

The following script gives initial guesses for the coefficients, and finds the best fit coefficients

```
Starting=[1.4 .5 .4];
options=optimset('Display','iter');
Estimates=fminsearch(@expfitradius,Starting,options,t,radii)
```

Power Law for Radius

Function powerradius returns the sum of error squared for coefficients

```
function [sse] = powerradius(params,Input,Actual_Output)
%fit of radius data to power function r(t)=C*t^n
%params should be an array of the form params=[re a T]
C=params(1);
n=params(2);
Fitted_Curve=C*Input.^n;
Error_Vector=Fitted_Curve-Actual_Output;
%sum of squares error
sse=sum(Error_Vector.^2);
end
```

The following script gives initial guesses for the coefficients, and finds the best fit coefficients

```
Starting=[1.4 .03];
options=optimset('Display','iter');
Estimates=fminsearch(@powerradius,Starting,options,t,radii)
```

Exponential Fit for Contact

Function expfitcontactangle returns the sum of error squared for coefficients

```
function [sse] = expfitcontactangle(params,Input,Actual_Output)
%fit of contact angle data to exponential function theta(t)=thetae-
b*exp(-t/T)
%params should be an array of the form params=[re a T]
thetae=params(1);
b=params(2);
T=params(3);
Fitted_Curve=thetae-b.*exp(-1/T*Input);
Error_Vector=Fitted_Curve-Actual_Output;
%sum of squares error
sse=sum(Error_Vector.^2);
end
```

The following script gives initial guesses for the coefficients, and finds the best fit coefficients

```
Starting=[63 -20 .25];
options=optimset('Display','iter');
Estimates=fminsearch(@expfitradius,Starting,options,t,theta)
```

Appendix C: Tips for future research

For future research in the spreading of trisiloxane surfactants, I will provide the following tips:

- Use either a high-resolution camera, or a larger lighting source and decrease the aperture of the camera as much as possible. Inconsistencies in the data and failure of the code to correctly detect circles at some points was due to the pictures being slightly blurry, and Matlab having trouble with edge detection.
- Have a device that holds the pipette in place at a set distance as oppose to manually holding it. It was hard to get good samples when manually holding the pipette, as my hands were shaky sometimes. In addition, a device holding the pipette would allow for it to be raised just enough to prevent the formation of capillaries, but not enough to allow any inertial effects to build up. This may alleviate problems with having drops start at different radii and contact angles.

6. Bibliography

Nikolov, A., & Wasan, D. (2011). *Superspreading Mechanisms: An Overview.* Department of Chemical Engineering. Chicago: Illinois Institute of Technology.

Radulovic, J., Sefaine, K., & Shanahan, M. E. (2009). *Dynamics of Trisiloxane Wetting: Effects of Diffusion and Surface Hydrophobicity.* Institute for Materials and Processes, School of Engineering. Edinburgh: The University of Edinburgh.

Schlumberger. (2007). *Technical Paper: Application of a Viscoelastic Surfactant-Based CO2 Compatible Fracturing Fluid in the Frontier Formation, Big Horn Basin, Wyoming.* Retrieved 4 5, 2012, from Schlumberger Resources: http://www.slb.com/resources/technical_papers/industry_challenges/unconventional_gas/107966.aspx

Schramm, L. L. (2000). *Surfactants: Fundamentals and Applications in the Petroleum Industry.* Petroleum Recovery Institute. Cambridge: Cambridge University Press.